The Deuterium, Oxygen, and Nitrogen Abundance Toward LSE 44

S.D. Friedman, (STScI), G. Hebrard (IAP), T.M. Tripp (UMass), P. Chayer (JHU), K. Sembach (STScI)

SPACE TELESCOPE SCIENCE INSTITUTE

Operated for NASA by AURA

Introduction

Precise measurements of primordial abundances of the light elements deuterium (D), ^{3}He, ^{4}He, and ^{7}Li relative to hydrogen have been a goal of astronomers for many years. In the standard Big Bang nucleosynthesis model, these quantities are related in a straightforward way to the baryon-to-photon ratio in the early universe, from which Ω_B, the fraction of the critical density contributed by baryons, may be determined (Boesgard & Steigman 1985). In the local interstellar medium (ISM) and throughout the Milky Way, the effects of astration, supernovae, stellar winds, infall of low metallicity material, and mixing have modified D/H. An important goal of FUSE has been to investigate the distribution of deuterium, oxygen, and nitrogen, and to place constraints on models of galactic chemical evolution and models which attempt to account for mixing of this material on various spatial and temporal scales.

We present results of an analysis of the sight line toward LSE 44, a subdwarf O star located at a distance of 554 ± 66 pc in the direction (l,b) = (313°,+13°). It was observed with *FUSE* for approximately 86 ksec over eight visits between April 2002 and Feb. 2004, in timetag mode using the MDRS spectrograph aperture. The data were reduced using CALFUSE pipeline version 3.0.6. 119 separate exposures were scheduled, but not all were successful. The useful exposures were cross-correlated, shifted, and co-added, resulting in a final spectrum with resolution of ~20 km sec^{-1} (FWHM), and S/N ~26 in the SiC1B channel. Several properties of the LSE 44 and the sight line are given in Table 1. The spectrum from channel segment SiC1B is shown in Figure 1.

In this study, we derive DI, OI, and NI column densities with data obtained from *FUSE*, and the HI column density with data from *IUE*.

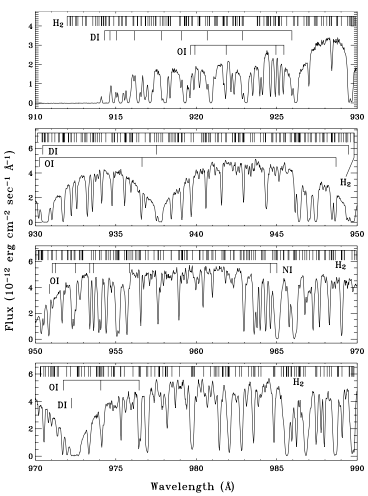

Figure 1. The SiC1B spectrum of LSE 44. Lines of interstellar DI, OI, NI, and H_2 are indicated.

Quantity	Value	Reference
Spectral Type	sdO	1
(l,b)	(313°.37, +13°.49)	
d (pc)	582 ± 66	2
z (pc)	129 ± 15	2
V	12.45	1
$U-B$	-1.18	1
$B-V$	-0.24	1
E_{B-V}	0.05 ± 0.03	2
T_{eff}	38700 ± 1000	2
log g (cm s^{-2})	5.5 ± 0.1	2
log [N(He)/N(H)]	−2.8 ± 0.1	2

References. — (1) Drilling, J.S. 1983, ApJ, 270, L13. (2) This study.

Table 1. Target and sight line parameters for LSE 44.

Stellar Properties and Stellar Model

LSE 44 displays a complex far-ultraviolet spectrum. The strong Lyman series lines of HI (Lyβ up to Ly7) are the dominant stellar features. The strongest photospheric metal lines are the NIV λ923 sextuplet, SVI λ933 and 944 doublet, NIV λ955, NIII λ979.9 quadruplet, NIII λ989.80, 991.51, and 991.58 triplet, NIII λ1006, HeII λ1084, PV λ1118 and 1128 doublet, SiIV λ1122 and 1128 triplet, CIII λ1175 sextuplet, and NIII λ1183 and 1184 quadruplet. We identified many strong ISM lines superimposed on the stellar spectrum. We were unable, however, to identify many remaining photospheric lines due to lack of reliable atomic data.

We observed LSE 44 at the South African Astronomical Observatory and obtained an optical spectrum that covers a wavelength range of 3400-5400 A with a resolution of about 3 Å and a signal-to-noise of ~100. To measure the atmospheric parameters of LSE 44, we fitted the Balmer lines with a grid of NLTE H+He atmospheres models that we computed by using the programs TLUSTY/SYNSPEC (see, e.g., Hubeny & Lanz 1995, ApJ, 439, 875). We obtained Teff = 38700 ± 1000 K, log g = 5.5 ± 0.1, and log(He/H) = -2.8 ± 0.1.

HI Column Density Analysis

The Lyα line provides the best constraint on the total HI column density because its radiation damping wings are very strong. To measure the total interstellar HI column density, we used the Lorentzian wings of the Lyα profile (Jenkins 1971), which have optical depth at wavelength λ given by $\tau(\lambda) = N(HI)\sigma(\lambda) = 4.26 \times 10^{-20} N(HI)(\lambda - \lambda_0)^{-2}$. Here λ_0 is the centroid of the interstellar HI absorption. We estimated the value of N(HI) that provides the best fit to the Lyα profile by minimizing χ^2 with five free parameters: N(HI), 3 coefficients that fit a second-order polynomial to the continuum (with a model stellar Lyα line superimposed), and a correction for the flux zero level (Jenkins et al. 1999).

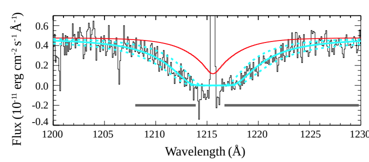

Figure 2. The *IUE* Lyα spectrum of LSE 44. The blue solid line is the best fit interstellar HI profile. Dotted lines indicate the 2σ upper and lower bounds. The gray horizontal lines indicate the regions of the spectrum used in the fit; additional spectral regions outside the plot are also used. The orange line is the stellar model based on the optical and FUV data. The emission line in the center of the saturated core is geocoronal Lyα emission.

H_2 Column Density Analysis

We used a COG analysis to measure the populations of molecular hydrogen in the J=2 to J=5 states, as shown in Figure 3. Observed J=0 and 1 lines are saturated, and accurate column densities could not be determined. Determining column densities for the J=2 and 5 states was required to deblend them from the weak OI λ974.070 line, which was used to determine the OI column density.

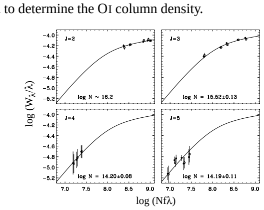

Figure 3. Curves of growth for H_2 J=2-5. All curves are plotted over the same range of log(Nfλ) to clearly display the rotational levels for which N(H_2) is well constrained.

Quantity	Value (2σ errors)
log N(D I)	15.87 ± 0.08
log N(O I)	$17.57\,^{+0.21}_{-0.15}$
log N(N I)	16.43 ± 0.14
log N(H I)	$20.52\,^{+0.20}_{-0.36}$
D/H	$(2.24\,^{+1.39}_{-1.32}) \times 10^{-5}$
O/H	$(1.13\,^{+0.96}_{-0.71}) \times 10^{-3}$
N/H	$(8.13\,^{+3.09}_{-2.24}) \times 10^{-5}$
D/O	$(1.99\,^{+1.30}_{-0.67}) \times 10^{-2}$
D/N	$(2.75\,^{+1.19}_{-0.89}) \times 10^{-1}$

Table 3. Summary of results from this study.

DI, NI, and OI Column Density Analyses

The DI and NI column densities were determined using the profile fitting code Owens.f. For deuterium, 5 lines in the SiC1B and SiC2A channels were fit simultaneously, and 6 lines for nitrogen. The continuum shape, zero flux level, and line spread function varied between windows, but the DI column density, radial velocity, and temperature were constrained to a common value, and similarly for NI. Examples of profiles fits are shown in Figure 4. Although we show only 4 windows, the complete fits include ~60 windows and 100 transitions. Our best estimates of the column densities are log N(DI) = 15.87 ± 0.08 and log N(NI) = 16.43 ± 0.14 (2σ errors).

The OI column density was estimated using two methods, curve of growth (COG) and profile fitting. For the COG method we assumed a single interstellar cloud with a Maxwellian velocity distribution. We measured the equivalent widths (W_λ) of the OI lines after fitting low-order Legendre polynomials to the local continuum profiles, thus removing small residual flux discrepancies between the stellar model and the observed spectrum. Figure 5 shows the curve of growth for the DI lines. The measured equivalent widths are given in Table 2. The estimated errors include contributions from both statistical and fixed-pattern noise in the local continuum.

All OI lines except for λ974.070 are saturated, which causes uncertainty in the column density analysis, especially when there are significant uncertainties in the LSF and velocity structure of the absorption profiles. λ974.070 is weak, and required significant deblending with J=2 and J=5 lines of H_2, but provides the best constraint on N(OI). The best estimate of the OI column density when combining the profile fitting and COG results is log N(OI)=17.57 + 0.21 - 0.15 (2σ). It is worth noting that if the λ974.070 is excluded, the COG analysis gives log N(OI)=17.22 + 0.55 - 0.29, showing the importance of including unsaturated lines. This problem may be responsible for underestimated errors in the analyses of some sight lines.

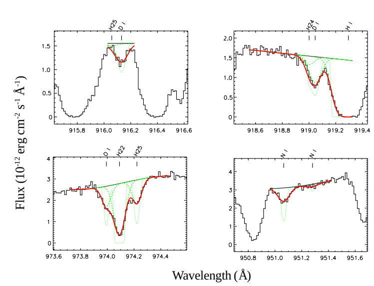

Figure 4. Profile fits of selected absorption lines. Histogram lines are the FUSE data. Solid black lines are the continua and solid red lines are the fits. The dashed green lines are the fits for each species. The dotted lines are the models prior to convolution with the LSF. H_2 lines in levels J=2, 4, and 5 are labeled H22, H24, and H25.

Discussion

The principal results of this study are listed in Table 3 and in Figure 6, which displays D/H vs. the HI column density. This figure shows that D/H is uniform within the Local Bubble, where log N(HI) < ~19.2 (Moos et al. 2003), and highly variable at intermediate column densities. For distant sight lines having high column densities, log N(HI) > ~20.5, D/H appears uniform but with a low value, D/H ~ 0.9 x 10^{-5}, as indicated by the solid horizontal line in Figure 6. Hebrard & Moos (2003) suggest that this is the true present epoch Galactic value, based on measurements of D/O toward these targets, and previous studies of O/H (Meyer 2001). D/O toward LSE 44 is consistent with this result.

Drain (2004) has suggested that D may be partially depleted onto dust grains, thus giving rise to the observed variability in the *gas phase* measurements of D/H in Figure 6. Wood et al. (2004) and Linsky et al. (2006) have suggested that this variability is due to differing levels of depletion of deuterium. Nearby supernovae may shock grains, liberating D back into the gas phase. Turbulent mixing may homogenize some regions, which may explain the uniformity seen within the Local Bubble. If the depletion hypothesis is correct, then high measures of D/H, like that along the LSE 44 sight line, represent the Galactic value.

These competing viewpoints can be tested by correlating D/H with levels of depletion of refractory elements, such as Fe, Si, or Ti (Prochaska, Tripp, & Howk 2005). A successful model must explain the appropriate astration factors required to account for the transition from the primordial to the Galactic D/H value, as well as the apparent spatial uniformity of D/O and O/H, but the non-uniformity of D/H.

See Friedman et al., ApJ, 20 February 2006 for a complete description of this study.

λ(Å)	log λf	W_λ [mÅ] SiC1B	SiC2A	LiF1A	LiF2B
925.446	-0.484	74.4 ± 6.0	71.0 ± 4.5	···	···
971.738	1.128	112.3 ± 6.3	105.2 ± 6.4	···	···
974.070	-1.817	33.3 ± 4.8	34.3 ± 4.5	···	···
1039.230	0.974	···	···	122.0 ± 3.1	120.7 ± 3.8

Table 2. Measured equivalent widths of OI absorption lines.

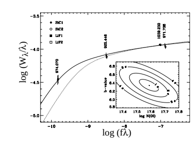

Figure 5. OI curve of growth. The best fit solution (solid line) is log N(OI) = 17.59 +0.15 -0.14 (2σ). If the λ919 line is excluded from the fit, the solution is log N(OI) = 17.22 +0.55 -0.29 (dotted line), more than 2.6σ below the best fit value. This shows that the lack of optically thin lines can lead to large errors in the column density estimate. For clarity, at each wavelength the data points derived from each FUSE channel have been slightly separated. The inset shows the log(N)/*b*-value error contours for the best fit solution.

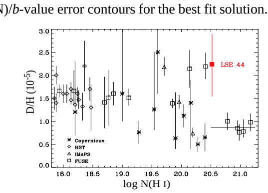

Figure 6. D/H as a function of the HI column density. LSE 44 is one of the few targets with high N(HI) that has a high value of D/H.

We thank Dave Kilkenny for providing the optical spectrum of LSE 44, and Gerry Williger for reducing it. This work is based on data obtained for the Guaranteed Time Team by the NASA-CNES-CSA *FUSE* mission operated by the Johns Hopkins University. Financial support has been provided by NASA contract NAS5-32985 and grants NNG04GH19G and NNG04GG73G. This work has used the profile fitting procedure developed by M. Lemoine and the FUSE French Team.